

High-performance thermoelectricity in quantum-Hall Corbino structures

Mariano Real,^{1,2} Daniel Gresta,³ Christian Reichl,⁴ Jürgen Weis,⁵ Alejandra Tonina,^{1,2}
Paula Giudici,⁶ Liliana Arrachea,³ Werner Wegscheider,⁴ and Werner Dietsche^{4,5}

¹*Instituto Nacional de Tecnología Industrial, INTI,
Av. Gral. Paz 5445, (1650) Buenos Aires, Argentina*

²*Instituto de Calidad industrial-UNSAM, Buenos Aires, Argentina*

³*International Center for Advanced Studies, ECyT-UNSAM,*

Campus Miguelete, 25 de Mayo y Francia, 1650 Buenos Aires, Argentina

⁴*Solid State Physics Laboratory, ETH Zürich, CH-8093 Zürich, Switzerland*

⁵*Max-Planck-Institut für Festkörperforschung, Heisenbergstrasse 1, D-70569 Stuttgart, Germany*

⁶*INN CNEA-CONICET, Av. Gral. Paz 1499 (1650) Buenos Aires, Argentina*

We study the thermoelectric response of Corbino structures in the quantum Hall effect using a resistive central heater. We present measurements of the thermoelectric voltage developed across the radius of the sample along with a theoretical analysis of these experiments. Our results indicate that the thermoelectric response is originated in the electrons, without effects introduced by the electron-phonon interaction. On this basis we estimate the figure of merit of the device and we show that it is very promising for a high-performance thermoelectrical cooling and heat-engine operation, particularly for partially filled Landau levels and high magnetic fields.

Introduction. The quantum Hall effect (QHE) is one of the most prominent examples of synergy between fundamental physics and quantum technologies [1]. It is topological in nature and intrinsically related to exotic properties of matter, like fractionalization and non-abelian statistics [2–4]. At the same time, are precisely these complex properties the reason for its robustness and appealing for practical applications. It is nowadays at the heart of the definition of the electronic metrological standards [5–8], while it is also a promising platform for the development of topological quantum computation [9].

Boosting the thermoelectric performance in the quantum regime is a very active avenue of research for some time now [10–12], which is receiving increasing interest in the context of the QHE. After experimental works on heat transport along edge states [13–18], characteristics like chirality [20–23], interference [25, 26], and fractionalization [27] were identified in theoretical works as promising to enhance the thermoelectric performance. A key ingredient for thermoelectric mechanisms is the existence of energy filters and the consequent breaking of particle-hole symmetry. The spectrum of the bulk of a two dimensional electron systems (2DES) in the QHE regime is characterized by Landau levels separated by an energy gap, which provides an appropriate scenario in this sense. In fact, the implementation of thermoelectric cooling based on this property has been proposed in Ref. [28] and, more recently, in Dirac systems in the quantum Hall state [29]. Thermoelectric effects might be also useful to better understanding fundamental properties of 2DES in the QHE regime, like the existence of neutral edge states in fractional filling factors [30, 31], and to probe the non-abelian nature of the $\nu = 5/2$ state through the relation between thermopower and entropy [32–35].

The aim of the present work is to analyze the ther-

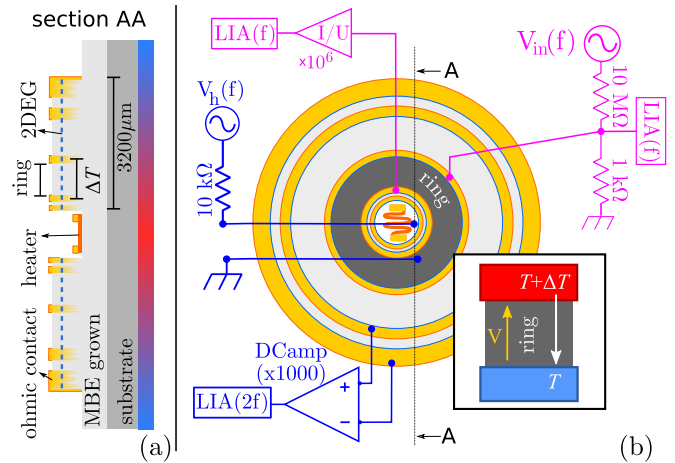


FIG. 1. Scheme of experimental setup. (a) A cross-section of the sample is included (a), notice that the heater element is over the substrate outside the 2DES. (b) Measurement configurations for the conductance and the thermovoltage are shown in light-grey (magenta online) and black (blue online), respectively. LIA denotes lock-in amplifier. A sketch of the effective transport description is indicated at the bottom.

moelectric response with a focus on the performance of a 2DES of a GaAs-AlGaAs heterostructure in the QHE regime with Corbino geometry, as a function of the magnetic field, covering a wide range of filling factors. We will show that this device has the potential for implementing high-performance thermoelectricity, qualified by a high figure of merit ZT [10–12]. Due to the circular shape of Corbino structures, the voltage and thermal biases are applied radially, hence, thermal and electrical transport is induced along this direction [36–40]. The edge states are not expected to play any essential role and the transport takes place through the bulk Landau levels.

The setup we study is sketched in Fig. 1. A metallic

island (heater) is inserted in the center of the Corbino sample. This is heated up by Joule effect with an AC current of low frequency f , such that the relaxation time of the electrons is much faster than $1/f$ [34, 35, 41, 42]. In this way, a radial thermal gradient is induced between the center and the external edge of the sample, which is assumed to be at the temperature T of the bath. As a response to the thermal bias, an electrical flow across the structure with the concomitant charge accumulation in the inner and outer circumferences generates a voltage with an oscillating component of frequency $2f$. The thermoelectric response in this device is much simpler than the one in the Hall bar geometry, where the transport takes place along longitudinal and transverse directions with respect to the applied biases. In fact, in the Corbino geometry, the thermovoltage develops along the direction of the temperature bias. This enables a clear assessment of the relevant transport mechanisms.

Experimental setup. The samples were grown by molecular beam-epitaxy on GaAs wafers having a single 2DES by means of a quantum well with two silicon doped layers. They were microprocessed with standard optical lithoprocessing and etching, producing a ring-shaped mesa. Ohmic contacts were produced by alloying Au-Ge-Ni into the heterostructure, creating several concentric rings ranging from 0.4 mm to 3.2 mm, while a central AuPd heater, outside the mesa, was also evaporated in another process. The response of the four concentric Corbino rings is assumed to be independent during the measurements. In the present text we will only show results for the *ring* which is highlighted in Fig. 1. Several samples were studied, the one presented in this letter has a mobility of $20.60 \times 10^6 \text{ cm}^2 \text{ V}^{-1} \text{ s}^{-1}$ and an electron density of $n_e = 3.065 \times 10^{11} \text{ cm}^{-2}$ at 1.3 K in the dark. These values were further confirmed by $1/B$ Shubnikov de Haas (SdH) oscillations on Corbino measurements. In the supplementary material (SM), Ref. [43], we also discuss results for some other samples and rings. In all cases the samples were glued in a standard commercial ceramic holder with gold-plated pins and base, a 3 mm diameter hole drilled in the middle reduce thermal contact to the samples. The measurements were performed in a ^3He cold finger cryostat being able to achieve a base temperature of 250 mK, it also posses a 14 T superconducting magnet.

Fig. 1 shows the setup configuration used for the measurements of the conductance (light-gray, magenta online) and the thermovoltage (black, blue online). *a)* The conductance G was measured by applying an AC voltage through a voltage divider. The output is measured with a lock-in amplifier (LIA). A characterized current to voltage amplifier (IUamp) was used to measure the current through the device. *b)* Thermovoltage V_{tp} measurements were performed applying an AC voltage V_{in} of frequency f to the resistive sample heater by means of a LIA output, the thermopower induced in the sample was then

measured by using a fixed $\times 1000$ differential DC voltage amplifier (DCamp)[50]. In all cases the time reference of the measurements was given by the same LIA (not shown in the figure). To avoid effects of time-dependent magnetic fluxes, the waiting time for each measurement point was set to guarantee the stabilization of the magnetic fields at a constant value. Special care was taken in the selection of both the IUamp and the DCamp. Further discussion on these points is presented in the SM, Ref. [43].

Thermoelectric response. We consider the sketch at the bottom of Fig. 1 to describe the thermoelectric transport. The ring acts as a conductor between hot and cold reservoirs with a temperature bias ΔT imposed by the heater. In linear response, the corresponding charge and heat currents for small ΔT and bias voltage V can be expressed as[11]

$$\begin{pmatrix} I^C/e \\ I^Q \end{pmatrix} = \begin{pmatrix} \mathcal{L}_{11} & \mathcal{L}_{12} \\ \mathcal{L}_{21} & \mathcal{L}_{22} \end{pmatrix} \begin{pmatrix} X_1 \\ X_2 \end{pmatrix}, \quad (1)$$

where $X_1 = eV/k_B T$ and $X_2 = \Delta T/k_B T^2$ and $\hat{\mathcal{L}}$ is the Onsager matrix. The electrical and thermal conductances are, respectively, $G = e^2 \mathcal{L}_{11}/T$, and $\kappa = \text{Det} \hat{\mathcal{L}} / (T^2 \mathcal{L}_{11})$. $S = \mathcal{L}_{12}/\mathcal{L}_{11}$ defines the Seebeck and $\Pi = \mathcal{L}_{21}/\mathcal{L}_{11}$ is the Peltier coefficient. For ballistic or diffusive transport \mathcal{L}_{ij} depends only on the quantum dynamics of the electrons in the presence of the magnetic field and the disorder of the sample. They are described by a transmission function $\mathcal{T}(\varepsilon)$,

$$\mathcal{L}_{ij} = -T \int \frac{d\varepsilon}{h} \frac{\partial f(\varepsilon)}{\partial \varepsilon} (\varepsilon - \mu)^{i+j-2} \mathcal{T}(\varepsilon), \quad (2)$$

where $f(\varepsilon) = 1/(e^{(\varepsilon-\mu)/k_B T} + 1)$ is the Fermi distribution function, μ is the chemical potential and T is the temperature of the electrons[44]. In the presence of disorder and absence of electron-electron interactions $\mathcal{T}(\varepsilon)$ was originally calculated by Jonson and Girvin[45]. At high temperatures, electron-phonon interaction gives rise to an additional component to the transport coefficients \mathcal{L}_{ij} . The corresponding thermopower has been studied in bar geometries for specific filling factors[47, 48] and, more recently, in illuminated Corbino samples[49], while no signatures of electron-phonon interaction were found in other experimental works in the Corbino geometry [46]. The thermal conductance has an additional component of purely phononic origin. We do not have access to this transport coefficient with the present experimental setup.

Conductance and thermovoltage. Our goal is to accurately describe the electronic component of the Onsager coefficients obtained from the experimental data. Applying a bias voltage V_{in} , we measure the conductance $G(B)$ as a function of the applied magnetic field B . The thermovoltage V_{tp} corresponds to the voltage for which

$I^C = 0$ in Eq. (1),

$$V_{tp}(B) = -S(B) \frac{\Delta T}{T}. \quad (3)$$

Here $S(B)$ is the Seebeck coefficient as a function of the magnetic field, T is the temperature of the bath (cold finger in our case) and ΔT is the temperature difference between the two edges of the Corbino ring under investigation. Since ΔT is a function of the supplied power, it has a component which slowly oscillates with a frequency $2f$. The corresponding oscillating component of the thermopower is recorded by the LIA (blue circuit of Fig. 1). More details are presented in Section I. B of the SM, Ref. [43]. From the data of $G(B)$ we infer the transmission function $\mathcal{T}(\varepsilon)$ entering Eq. (2). Given $\mathcal{T}(\varepsilon)$, we can evaluate the electrical component of the other Onsager coefficients, in particular $\mathcal{L}_{12}(B)$. Through Eq. (3), this leads to a theoretical prediction for the behavior of $V_{tp}(B)$ resulting from the electrical transport, which can be directly contrasted with the experimental data.

There are two regimes to be considered for the calculation of $\mathcal{T}(\varepsilon)$: (i) At low magnetic fields, where the different Landau levels are not clearly resolved, we calculate the transmission function with the model introduced in Ref. [33, 45]. The latter is based on a single-particle picture for the 2D electron gas in the presence of a magnetic field and elastic scattering introduced by impurities. (ii) For higher magnetic fields, where the different filled Landau levels are clearly distinguished, and separated by a gap, we use the fact that in the limit of $T \rightarrow 0$, Eq. (2) leads to $\mathcal{T}(\mu) \sim G(\mu)/e$. Details are given in the SM (see Section II.A of Ref [43]).

Results for the conductance and the thermovoltage are shown in Fig. 2 for the temperature 269 mK. The experimental data for G and V_{tp} within the regime of low magnetic field is shown in the upper panel of the figure along with the theoretical description based on the transmission function of Eq. (5) of the SM, [43]. In the case of high magnetic field, shown in the lower panel, the theoretical description was based in the transmission function of Eq. (6) of the SM, [43]. Given $\mathcal{T}(\varepsilon)$, we calculate the Onsager coefficients of Eq. (2) and the Seebeck coefficient $S = \mathcal{L}_{12}/\mathcal{L}_{11}$. The ratio $\Delta T/T$ has been adjusted in order to fit the experimental measurements with Eq. (3). Details are presented in Sec. II.B of the SM, [43]. The estimates for the temperature bias were $\Delta T = 1$ mK and 1.08 mK, for low and high magnetic fields, respectively, which is of the correct order of magnitude of the experimental estimate, $\Delta T \sim (9 \pm 2)$ mK with the heater supplied with a dc source (see Section I.C of Ref. [43]). Overall, in particular for high magnetic fields, the agreement between experiment and theory is excellent within the range of B corresponding to partially filled Landau levels, for which $G \neq 0$. Interestingly, within the gap between Landau levels, for which $T\mathcal{L}_{11} = G \sim 0$, the thermovoltage achieves the largest

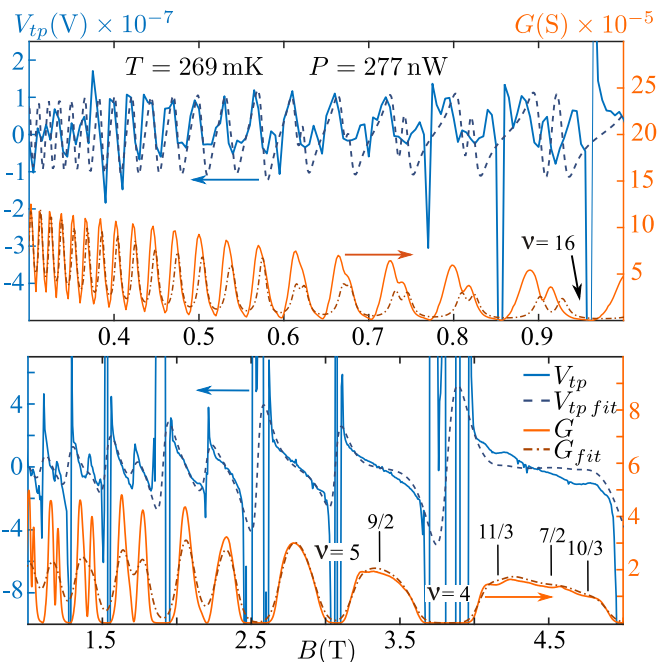


FIG. 2. Conductance G and thermovoltage V_{tp} as a function of the magnetic field B for the ring 2 in Fig. 1 at temperature T with power P supplied at the heater. Experimental data is plotted in solid lines. Theoretical (dashed) plots are based on the calculation of Eq. (2) with the inferred transmission function as explained in (i) and (ii) for the upper and lower panel, respectively.

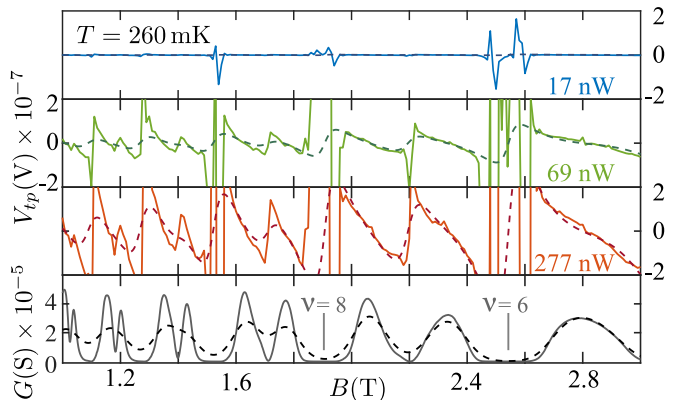


FIG. 3. Thermovoltage V_{tp} for a fixed temperature and different powers P' applied at the heater, assuming $\Delta T(P') = P'/P \cdot 1.08 \times 10^{-3}$ K. P and other details are the same as in Fig. 2.

amplitude. This behavior is smooth in the plots corresponding to the theoretical prediction while it is more abrupt and exhibits many features in the experimental data. Further study, beyond the scope of the present work is necessary here, since other effects like edge-state currents[51] or inhomogeneities[52, 53] might play a role.

Taking into account the good agreement between the

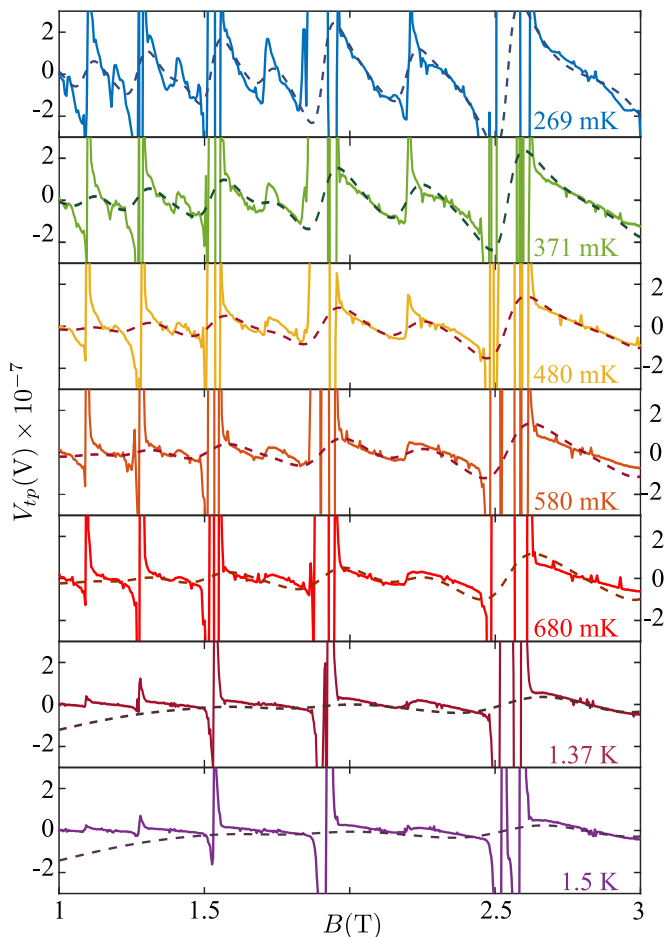


FIG. 4. Thermovoltage V_{tp} , as function of the magnetic field for different temperatures. In the case of 269 mK to 680 mK a power of 277 nW, while for 1.37 K to 1.5 K the heater power applied was 433 nW. Other details are the same as in previous Figs.

experimental and theoretical estimates of the temperature difference ΔT found in the analysis of the data of Fig. 2, we now analyze the relation between the electrical power supplied at the heater and ΔT . In Fig. 3 we show experimental data for the thermovoltage at a fixed temperature and different heater powers. We have assumed a linear dependence between these quantities. Therefore, we have fitted the experimental data with the same Seebeck coefficient $S(B)$ calculated for Fig. 2 and the following values of the temperature difference, $\Delta T(P') = P'/P 1.08 \times 10^{-3}$ K, being P' the power corresponding to the experimental data and P the power used in the data of Fig. 2. We see a very good agreement between the theoretical prediction and the experimental data.

In Fig. 4 we discuss the evolution of V_{tp} as the temperature grows, focussing on the high magnetic field region. As a reference, we also show in the lowest plot of the figure the conductance G measured at the lowest tem-

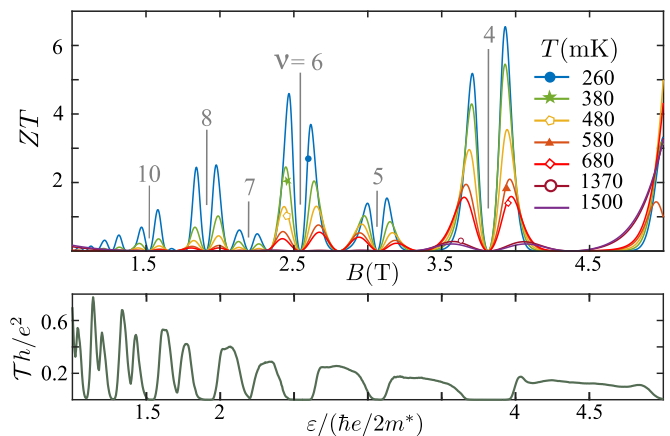


FIG. 5. Bottom: Transmission function $\mathcal{T}(\epsilon)$. Top: Electron contribution to the figure of merit ZT .

perature. The experimental data is presented along with the theoretical prediction obtained by following the same procedure of the previous Figs, and taking into account the linear dependence of ΔT with P explained in Fig. 3. The agreement between the theoretical predictions and the experimental data for magnetic fields corresponding to partially filled Landau levels within a wide range of temperature is overall very good, improving as the temperature decreases.

Thermoelectric performance. The quality of the thermoelectric performance is evaluated in terms of the efficiency (for the heat engine), or coefficient of performance (for the refrigerator), $\eta^{\text{he/fr}}$. Both coefficients can be parametrized by the figure of merit[11],

$$ZT = \frac{\mathcal{L}_{21}^2}{\text{Det}\hat{\mathcal{L}}}; \quad \eta = \eta^{\text{he/fr}} \frac{\sqrt{ZT+1}-1}{\sqrt{ZT+1}+1}. \quad (4)$$

such that the optimal Carnot limit $\eta_C^{\text{he/fr}}$ is achieved for $ZT \rightarrow \infty$, while $ZT \sim 3$ implies $\eta^{\text{he/fr}} \sim \eta_C^{\text{he/fr}}/3$. In Fig. 5 we show the transmission function $\mathcal{T}(\epsilon)$ used to fit the experimental data of Fig. 2 within the high-magnetic field regime. We see that the sequence of sharp features at the Landau levels realize energy filters, leading to large values of ZT . We stress that this analysis is based on the assumption that the main contribution to the thermoelectric and thermal transport is due to the electrons. Purely phononic thermal transport could tend to decrease the performance. Nevertheless, such an effect is expected to be small at the lowest temperatures analyzed here.

Conclusions. We analyzed the thermoelectric response of a Corbino structure in the quantum Hall effect. For partially filled Landau levels, we found an excellent agreement between the experimental data and the theoretical description based on the assumption that the thermoelectric response is originated in the transport of electrons in absence of electron-phonon interaction. We were able to

accurately estimate the difference of temperature generating the oscillating component of the thermopower. The calculated figure of merit ZT is remarkably high for high magnetic fields, indicating that this system is very promising as a low-temperature cooling device or a heat engine.

Acknowledgements We thank Klaus von Klitzing for his constant interest and support, Achim Güth and Marion Hagel for the wafer lithography, Peter Märki (ETH) for helpful discussions and providing the amplifiers used in this work, Lars Tiemann for the measurement software "Nanomeas" (www.nanomeas.com) and Peter Samuelsson for useful comments on the manuscript. We acknowledge support from INTI and CONICET, Argentina. We are sponsored by PIP-RD 20141216-4905 of CONICET, PICT-2017- 2726 and PICT-2018 from Argentina, Swiss National Foundation (Schweizerischer Nationalfonds) NCCR "Quantum Science and Technology", as well as the Alexander von Humboldt Foundation, Germany.

-
- [1] K. v. Klitzing, G. Dorda, M. Pepper, Phys. Rev. Lett. **45**, 494, (1980).
- [2] D. C. Tsui, H.L. Stormer, A. C. Gossard, Phys. Rev. Lett. **48** 1559 (1982).
- [3] R. B. Laughlin, Phys. Rev. Lett. **50** 1395 (1983).
- [4] J. K. Jain, Adv. Phys. **41**, 105 (1992).
- [5] A. Hartland, Metrologia **29**, 175 (1992).
- [6] W. Poirier, F. Schopfer, The European Phys. J. Special Topics. **172**, 207 (2009).
- [7] S. P. Giblin, M. Kataoka, J. D. Fletcher, P. See, T. J. B. M. Janssen, J. P. Griffiths, G. A. C. Jones, I. Farrer, D. A. Ritchie, Nat. Commun. **3**,930 (2012).
- [8] T. Gerster, A. Müller, L. Freise, D. Reifert, D. Maradan, P. Hinze, T. Weimann, H. Marx, K. Pierz, H. W. Schumacher, F. Hohls, N. Ubbelohde, Metrologia **56**, 014002 (2018).
- [9] C. Nayak, S. H. Simon, A. Stern, M. Freedman, S. Das Sarma, Rev. Mod. Phys. **80**, 1083 (2008).
- [10] F. Giazotto, F., T. T. Heikkilä, A. Luukanen, A. M. Savin, J. P. Pekola, Rev. Mod. Phys. **78** 2172006 (2006).
- [11] G. Benenti, G. Casati, K. Saito, R. S. Whitney, Phys. Rep. **694**, 1 (2017).
- [12] F. S. Bergeret, M. Silaev, P. Virtanen, T. T. Heikkilä, Rev. Mod. Phys. **90**, 041001 (2018).
- [13] G. Granger, J. P. Eisenstein, J. L. Reno, Phys. Rev. Lett. **102**, 086803 (2009).
- [14] Seung-Geol Nam, E. H. Hwang, Hu-Jong Lee, Phys. Rev. Lett. **110**, 226801 (2013).
- [15] S. Jezouin, F. D. Parmentier, A. Anthore, U. Gennser, A. J. Cavanna, F. Pierre, Science **342**, 6158 (2013).
- [16] V. Venkatachalam, S. Hart, L. Pfeiffer, K. West, and A. Yacoby, Nature Physics **8**, 676 (2012).
- [17] A. Cavanna, D. Mailly, F. Pierre, C. Altimiras, H. le Sueur, U. Gennser, A. Anthore, Phys. Rev. Lett. **109**, 026803 (2012).
- [18] M. Banerjee, M. Heiblum, A. Rosenblatt, Y. Oreg, D. E. Feldman, A. Stern, V. Umansky, Nature **545**, 75 (2017).
- [19] S. Akiyama, T. Hirasawa, Y. Sato, T. Akiho, K. Muraki, and T. Fujisawa, App. Phys. Lett. **115** 243106 (2019).
- [20] R. Sánchez, B. Sothmann, A. N. Jordan, Phys. Rev. Lett. **114**, 146801 (2015).
- [21] P. Roura-Bas, L. Arrachea, E. Fradkin, Phys. Rev. B **98**, 195429 (2018).
- [22] S. Kheradsoud, N. Dashti, M. Misiorny, P. P. Potts, J. Splettstoesser, P. Samuelsson, Entropy **21**, 777 (2019).
- [23] D. Gresta, M. Real, L. Arrachea, Phys. Rev. Lett. **123**, 186801 (2019).
- [24] P. P. Hofer, B. Sothmann, Phys. Rev. B **91**, 195406 (2015).
- [25] P. Samuelsson, S. Kheradsoud, B. Sothmann, Phys. Rev. Lett. **118**, 256801 (2017).
- [26] L. Vannucci, F. Ronetti, G. Dolcetto, M. Carrega, M. Sassetti, Phys. Rev. B **92**, 075446 (2015).
- [27] P. Roura-Bas, L. Arrachea, E. Fradkin, Phys. Rev. B **97**, 081104 (2018).
- [28] F. Giazotto, F. Taddei, M. Governale, R. Fazio, F. Beltram, New J. Phys. **9**, 439 (2007).
- [29] L. Fu, arXiv:1909.09506.
- [30] G. Viola, S. Das, E. Grosfeld, A. Stern, Phys. Rev. Lett. **109**, 146801 (2012).
- [31] A. Aharon-Steinberg, Y. Oreg, A. Stern, Phys. Rev. B **99**, 041302 (2019).
- [32] K. Yang, B. I. Halperin, Phys. Rev. B **79**, 115317 (2009).
- [33] Y. Barlas, K. Yang, Phys. Rev. B **85**, 195107 (2012).
- [34] W. E. Chickering, J. P. Eisenstein, L. N. Pfeiffer, K. W. West, Phys. Rev. B **81**, 245319 (2010).
- [35] W. E. Chickering, J. P. Eisenstein, L. N. Pfeiffer, K. W. West, Phys. Rev. B **87**, 075302 (2013).
- [36] V. T. Dolgoplov, A. A. Shashkin, N. B. Zhitenev, S. I. Dorozhkin, K. v. Klitzing, Phys. Rev. B **46**, 12560 (1992).
- [37] R. F. Kazarinov, S. Luryi, Phys. Rev. B **25**, 7626 (1982).
- [38] N. R. Cooper, B. I. Halperin, Chin-Kun Hu, I. M. Ruzin, Phys. Rev. B **55**, 4551 (1997).
- [39] E. Ahlswede, J. Weis, K. v. Klitzing, K. Eberl, Physica E **12**,165 (2002).
- [40] B. A. Schmidt, K. Bennaceur, S. Bilodeau, G. Gervais, L. N. Pfeiffer, K. W. West, Solid State Commun. **217**, 1 (2015).
- [41] L. W. Molenkamp, H. van Houten, C. W. J. Beenakker, R. Eppenga, C. T. Foxon, Phys. Rev. Lett. **65** 1052 (1990).
- [42] L. W. Molenkamp, T. Gravier, H. van Houten, O. J. A. Buijk, M. A. A. Mabe-soone, C. T. Foxon, Phys. Rev. Lett. **68** 3765 (1992).
- [43] See Supplementary Material to this letter.
- [44] In the evaluation of the Onsager coefficients we consider for the electrons the temperature T of the bath. Corrections to this temperature due to the power supplied at the heater are irrelevant in the linear response regime.
- [45] M. Jonson, S. M. Girvin, Phys. Rev. B **29**, 1939 (1984).
- [46] S. Kobayakawa, A. Endo, Y. Iye, J. Phys. Soc. Japan **82**, 053702 (2013).
- [47] B. Tieke, U. Zeitler, R. Fletcher, S. A. J. Wieggers, A. K. Geim, J. C. Maan, M. Henini, Phys. Rev. Lett. **76**, 3630 (1996)
- [48] J. Zhang, S. K. Lyo, R. R. Du, J. A. Simmons, J. L. Reno, Phys. Rev. Lett. **92**, 156802 (2004)
- [49] H. van Zalinge, R. W. van der Heijden, J. H. Wolter, Phys. Rev. B **67**, 165311 (2003)
- [50] P. Märki, B. A. Braem, T. Ihn, Rev. Sci. Instrum. **88**,

- 085106 (2017)
- [51] A. V. Kavokin, B. L. Altshuler, S. G. Sharapov, P. S. Grigoryev, A. A. Varlamov, The Nernst effect in Corbino geometry, PNAS **117**, 2846 (2020)
- [52] J. Martin, S. Ilani, B. Verdene, J. Smet, V. Umansky, D. Mahalu, D. Schuh, G. Abstreiter, A. Yacoby, Science **305**, 980 (2004)
- [53] N. d'Ambrumenil, R. Morf, Phys. Rev. Lett. **111**, 136805, (2013)

Supplemental material: High-performance thermoelectricity in quantum-Hall Corbino structures

Mariano Real,^{1,2} Daniel Gresta,³ Christian Reichl,⁴ Jürgen Weis,⁵ Alejandra Tonina,^{1,2}
Paula Giudici,⁶ Liliana Arrachea,³ Werner Wegscheider,⁴ and Werner Dietsche^{4,5}

¹*Instituto Nacional de Tecnología Industrial, INTI,
Av. Gral. Paz 5445, (1650) Buenos Aires, Argentina*

²*Instituto de Calidad industrial-UNSAM, Buenos Aires, Argentina*

³*International Center for Advanced Studies, ECyT-UNSAM,*

Campus Miguelete, 25 de Mayo y Francia, 1650 Buenos Aires, Argentina

⁴*Solid State Physics Laboratory, ETH Zürich, CH-8093 Zürich, Switzerland*

⁵*Max-Planck-Institut für Festkörperforschung, Heisenbergstrasse 1, D-70569 Stuttgart, Germany*

⁶*INN CNEA-CONICET, Av. Gral. Paz 1499 (1650) Buenos Aires, Argentina*

I. EXPERIMENTAL DETAILS

In the course of this work we studied samples from close to 10 different wafers which were grown with different layer structures and varied in density and mobility. The wafers were initially characterized using the van der Pauw technique before Corbino structures as shown in Fig. 1 of the main text were produced by photo-lithography. Measurements of the conductance and the thermovoltage were carried out at temperatures between 256 mK to 2 K. They showed the typical oscillatory behavior in magnetic field. If conductance data appeared inhomogeneous then the thermovoltage measurements frequently showed an irregular, noise-like behavior. In all samples, however, the thermovoltages showed a qualitative similar behavior.

Here we present some technical details on the measurements of the thermovoltage, and also on the experimental estimate of the temperature distribution in the sample.

A. Temperature distribution in Corbino devices

Thermoelectric voltages are a consequence of a temperature gradient along the electronic system. In a traditional experiment one end of a rectangular sample is clamped to a thermal bath while the temperature at the other end is increased leading to a homogeneous temperature distribution along the length of the sample. This design cannot be directly transferred to ring-shaped Corbino structures where the center of the ring should be heated and the rim be cooled. It turns out to be difficult to connect the outer rim of the Corbino to a thermal bath with a vanishing thermal resistance. Another issue is the high thermal conductivity of the substrate which leads to small thermal gradients at reasonable heater powers. In the work of Kobayakawa et al. Ref. 3 the center was connected to a thermal sink and a circular rf heater surrounded all of the Corbino ring. We use the more conventional approach, which consists in placing a central resistive heater and glueing the rims of the sample to a chip carrier which is thermally connected with the cold finger of the cryostat. Our samples are square ($4 \times 4 \text{ mm}^2$) wafer pieces on which the ring-shaped design is produced

by photo-lithography. A heater made of AuPd alloy is placed in the central area where the 2DES has been removed, see Fig. 1(a) of the main text. Several concentric rings are produced by alloying AuGeNi into the 2DES area. The edges of the samples are glued to a ceramic chip carrier with a central hole leaving the inner 3.5 mm of the sample exposed.

An important assumption of this experiment is that the temperature at any point of the 2DES is equal to the one of the substrate which is determined by the heat conductivity of the substrate phonons. This approach follows the one of Chickering et al. Ref. 4 who showed that the substrate phonons determine the temperature gradient even at much lower temperatures. In our temperature range (0.3 K to 2 K) the heat conductivity is higher and the electron relaxation rates are even faster, thus the substrate phonons should be even more dominant in determining the radial temperature gradient experienced by the electrons.

There are some issues originating from the phonon heat conductivity in the substrate. One of them is that the phonon mean free path is of the order of the wafer thickness (0.5 mm) meaning that the usual assumption of a diffusive heat flow is only approximately correct. Another one is the anisotropy of the phonon propagation due to the crystal structure, also known as phonon focusing effect. This anisotropy becomes only significant if the phonon source is much smaller than the size of the sample. Our heater covers an area of about $500 \mu\text{m}$ in diameter, which should be large enough to keep distortions of the temperature distribution of the electrons small.

A consequence of the high phonon heat conductivity in GaAs is that the temperature differences between the center and the edges are small. Typical values are of the order of 1 mK as can be estimated from using the magnetoresistance values as thermometers (see section IC) and also from the fit of the thermoelectricity theory to the experimental data (see main text). On the other hand, there is a sizable temperature resistance between the sample and the cold plate of the cryostat. Thus, the temperature gradient on the wafer surface is always accompanied by a general temperature increase of the wafer as a whole. We have run temperature simulations using

Comsol and find that there is always a Gaussian-like temperature distribution near the heater. Near the edges the temperature profiles depend on the respective thermal resistance at the edges. Thus thermoelectric data from the outer rings are expected to be less reliable.

B. Measurement of the thermovoltage

As already explained in the main text, an AC current $I(t)$ of frequency f is applied to the heater

$$I(t) = I_0 \sin(\Omega t + \varphi), \quad (1)$$

with $\Omega = 2\pi f$, and φ a possible arbitrary phase. This translates into the power,

$$P(t) = \frac{RI_0^2}{2} [1 - \cos(2\Omega t + 2\varphi)], \quad (2)$$

where R the resistance of the heater.

Thus, a temperature bias is generated between the heater and the external rim of the structure which has a constant component and one that oscillates with the frequency $2f$. In Section IC, we will show that there exists a linear relation between the power and the temperature bias. Therefore, it is natural to assume the following behavior for the temperature bias,

$$\Delta T(t) = (\Delta T)_0 - (\Delta T)_2 \cos(2\Omega t + 2\varphi). \quad (3)$$

At very low frequencies and under ideal conditions, $(\Delta T)_2$ should be independent of the frequency and equal to $(\Delta T)_0$. Consequently, the developed thermovoltage has a constant component plus an oscillating component of frequency $2f$, i.e.

$$V_{tp}(t) = V_{tp,0} - V_{tp,2} \cos(2\Omega t + 2\varphi). \quad (4)$$

The experimental setup is designed to measure the oscillating component $V_{tp,2}$ of the thermovoltage. The Seebeck coefficient $S = \mathcal{L}_{12}/\mathcal{L}_{11}$ relating the thermovoltage with ΔT – see Eq. (3) of the main text – depends on the microscopic mechanisms behind the transport processes. Within linear response this quantity is the same for the constant and oscillating components of ΔT and V_{tp} . Notice that in this type of measurement there is a phase lag equal to $3\pi/2 + \varphi$ between the oscillations of the injected current and the measured thermovoltage. In all the Figs. we show in the main text and in this Supplementary Material, the injected signal has $\varphi = 0$ and the corresponding 2nd harmonic in the signal of V_{tp} has a phase lag of $3\pi/2$ within the Landau levels, in full agreement with Eqs. (1) and (4). However, within the gaps between Landau levels the response shows spike like voltages, which have also other phase lags. The origin of the latter feature is not yet clear and deserves future investigation.

From the technical point of view, it is important to chose the proper frequency range. We studied the thermopower response at different frequencies and found an

upper limit at $f = 100$ Hz, i.e. $2f = 200$ Hz where the voltage started to decrease with increasing frequency. On the other hand, the total cryosystem has a characteristic thermal-relaxation corresponding to a frequency below 2 Hz. These two frequencies determine the frequency range that could be used during thermopower measurements, we chose 13.8 Hz. The conductance measurements were not constrained by these limits because the additional power dissipation was always negligible. A higher frequency of 113 Hz increased the accuracy and reduced the measurement times, which was particularly relevant for the temperature calibration, to be discussed in section IC. In the QHE regime the internal resistance of the thermal voltage can become very high. Its measurement requires a DC amplifier with very high input impedance. We use an amplifier with about $10 \text{ T}\Omega$ input impedance and differential guarded inputs¹.

We verified that the measurement of the voltage across the radius of the device is indeed generated by a thermoelectric effect rather than being induced by a time-dependent magnetic field. The latter effect would actually be the experimental realization of Laughlin's *gedanken* experiment². According to this, a time-dependent magnetic flux threading the Corbino structure would induce an electrical field (induced emf by Faraday law) causing eddy currents circulating along the circumferences of the structure, which would lead to the development of a radial Hall voltage. This voltage would depend on the time-derivative of the magnetic field. Thus, the measurements have been performed by changing the magnetic field in steps using different waiting times to allow the thermovoltages to stabilize. In addition, we made voltage measurements in the thermovoltage configuration (see Fig. 1 of the main text) both within the Landau levels and within the gapped regions with the magnetic field pointing in opposite orientations. We did not find any signature of an effect due to a time-dependent magnetic flux.

As mentioned in the main text, we can distinguish two regimes in the behavior of V_{tp} as a function of the magnetic field as illustrated in the two panels of Fig. SM.1. For low magnetic fields (below 1 T), V_{tp} oscillates with magnetic field between positive and negative values as shown in the left panel. At higher magnetic fields (right panel), the quantum Hall effect (QHE) develops and the conductance minima tend to be vanishing small. Outside of these minima the thermovoltage still oscillates between positive and negative values but requires a different theoretical modeling as will be described in detail in Section II of this Supplementary Material. In the minima themselves large spike-like voltages are observed which are also related to the temperature gradient but have a varying phase with respect to the heater frequency. Its origin is not clear at this time. In the previous experiment by Kobayakawa et al. Ref. 3 this feature was not visible. Note that at even higher magnetic fields the spikes split into many noise-like but reproducible features, while the behavior between the QHE states still appears regu-

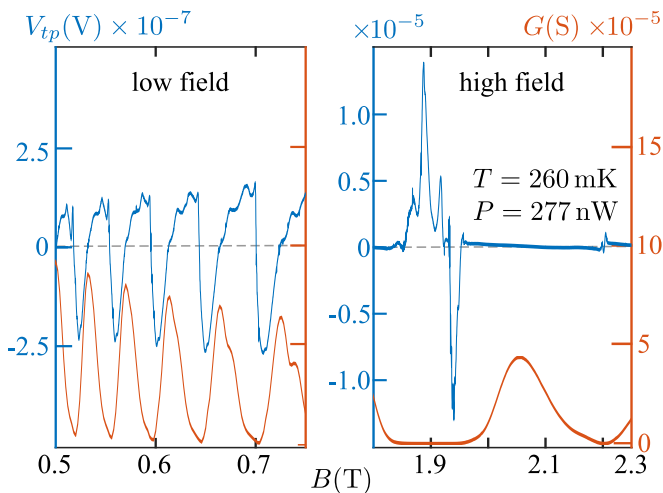


FIG. SM.1. Left axis, high-resolution V_{tp} response (blue online), right axis conductance measurements (orange online). Here measurements were produced under the same conditions as described in the main text but using much smaller magnetic field steps. In the left panel the magnetic field is too small to reach quantization. As soon as the conductance tends to zero at higher fields in the right panel, the spike-like thermal voltages develop.

lar. These spike-signals varied in magnitude from sample to sample. They could be due to incompressible areas (stripes) in the QHE state⁷ and also effects like edge-states currents could play some role.⁸ Such mechanisms cannot be described by the diffusion of quasi-particles. The chaotic behavior at very high magnetic fields may be caused by the splitting of the incompressible stripes in different ones. Inhomogeneities may also enhance this chaotic behavior. We added inhomogeneities by grinding samples to smaller thicknesses reducing the phonon conductivity. This led to a much more irregular behavior in the thermal voltage measurements, probably because of the stresses applied to the wafer during the grinding procedure. Such samples showed frequently an irregular behavior also in the compressible regimes of a magnetic field sweep.

In Fig. SM.2 we show the data for the thermovoltage measured across the different rings in another sample. We find similar features for all rings, albeit with different amplitudes which reflect the respective ΔT in each case. The radii of the different rings are : 400 μm to 500 μm ring 1, 600 μm to 1600 μm ring 2 , 1800 μm to 2600 μm ring 3 and 2800 μm to 3200 μm ring 4. Rings 2 and 3 have a larger width and therefore a larger ΔT and show larger thermovoltages than ring 4. Following a similar procedure as in the main text, we can estimate the second harmonic contribution to ΔT for the several rings. For the ring 2 we obtain $(\Delta T)_2 = (60 \pm 3) \mu\text{K}$, while for the ring 3 we get $(\Delta T)_2 = (110 \pm 10) \mu\text{K}$ and for ring 4 $(\Delta T)_2 = (74 \pm 50) \mu\text{K}$. All these measurements were made at a bath temperature of 600 mK and a power of 213 nW. These values are considerably lower than the

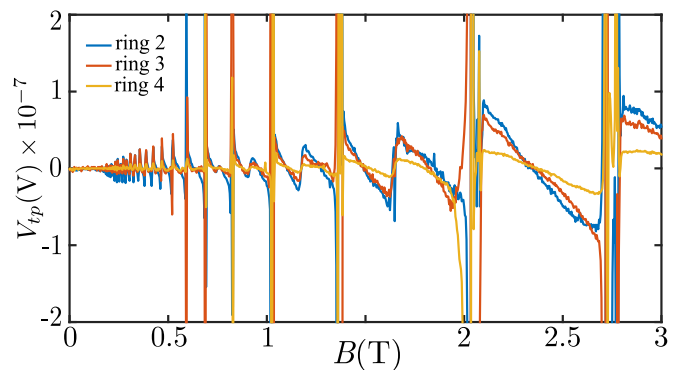


FIG. SM.2. V_{tp} response of sample B, this sample has a $17.5 \times 10^6 \text{ cm}^2 \text{ V}^{-1} \text{ s}^{-1}$ mobility and $2.03 \times 10^{11} \text{ cm}^{-2}$ density. Here measurements were made at different rings at a bath temperature of 600 mK and a heater power of 213 nW. Notice the difference between voltages on the rings, since ring 2 and ring 3 have a larger width than ring 4 they present a greater temperature gradient and hence a larger voltage response.

ones of the sample in the main text. However, they are perfectly consistent with those estimates. In fact, notice that the thermal conductivity of the substrate increases with T^3 and at 600 mK the temperature gradient will be almost 10 times smaller than at the measurement of the main text and a much smaller temperature difference is expected at the higher temperature.

C. Determining the local temperatures of the Corbino rings and estimating ΔT

The temperature sensitivity of the magneto-conductance of the different rings was used to provide an independent estimate of their respective temperatures and the temperature gradients through the sample. In a first step the conductances were calibrated against the Cernox thermometer of the cold finger without any power applied on the central heater. In a second step, power was applied to the central heater and the resulting temperature changes of the different rings were monitored. This procedure is similar to the one used by Chickering et al.⁴ for Hall-bars. Specifically, we used the configuration of Fig. SM.3, and we measured the conductance at Corbino rings 1 and 4 by applying an AC voltage (113 Hz) to one of the contacts and measure the current at the other using an IU amplifier and LIA. The conductance minimum at the $\nu = 9$ filling factor was used because it showed a clear temperature dependence.

The heater-off measurements were performed at bath temperatures (cold finger) between 267 mK and 600 mK. Heat was applied from a DC power supply, a source-measure unit (SMU), introducing a temperature gradient in the sample and the conductance of the Corbino rings was recorded at different heater powers as function of the bath temperature. The results – see Fig. SM.4 –

show that the temperature range below $T = 0.5$ K is useful because there is a monotonous relation between temperature and conductance for all power level.

Now the mean local temperatures $T_{\text{ring } j}$ of both rings $j = 1, 4$ at any bath temperature T and a heater power P can be inferred from the plots of Fig. SM.4 by starting from the corresponding value of $G(P, T)$ and drawing a horizontal line until intersecting the heater-off trace. The temperature difference $T_{\text{ring } 1} - T_{\text{ring } 4}$ can be determined from the local temperatures at the two rings. It turns out that this difference is indeed very small compared to the overall temperature rise of the wafer making its exact determination difficult. We used the highest possible precision like equilibrating the bath temperatures over at least 10 minutes to within less than 1 mK after each temperature change. Each measurement was repeated and averaged 20 times. The inset of the Fig. SM.4 shows the raw data for ring 1 and power 277 mW. We see that sweeping over the whole temperature range at a given power takes about 3 hours. Nevertheless, we were only able to obtain order of magnitude values for the temperature differences. To remove systematic variations which seem to depend on temperature, we averaged the results over a temperature range of 260 to 550 mK and obtained the dependence of the difference $T_{\text{ring } 1} - T_{\text{ring } 4}$ as function of power. It is plotted in Fig. SM.5 and we see that it is linear. The error bars indicate only the statistical errors of the averaging.

In the main text we obtained a temperature gradient of 1 mK from fitting the theoretical behavior of the thermovoltage to the data of ring 2 at a power of 277 nW and a bath temperature of 267 mK. The temperature difference across ring 2 can be estimated from the data in Fig. SM.5 using a linear approximation of the temperature profile to be about 9 mK. This is larger than the fit value but we consider it satisfactory with regard to the problems of measuring the temperature profile using magnetotransport data.

Alternatively one can also estimate the temperature profile using literature values of the thermal conductivity κ . From the work of Chickering et al.⁴ we deduced a κ of about 0.01 W/mK at 300 mK. Using the simulation software Comsol a temperature difference of 2.5 mK was found between the center and edge of our sample from the heat-flow equation. This would lead to a temperature difference across ring 2 of about 1 mK in good agreement with the value of the thermovoltage theory fit.

II. MODELING THE DATA

A. Transmission function $\mathcal{T}(\varepsilon)$

As mentioned in the main text, we model the experimental data by assuming that the transport coefficients are described by the response of the electrons, without the effect of electron-phonon interaction. This implies that all the transport coefficients, in particular, the

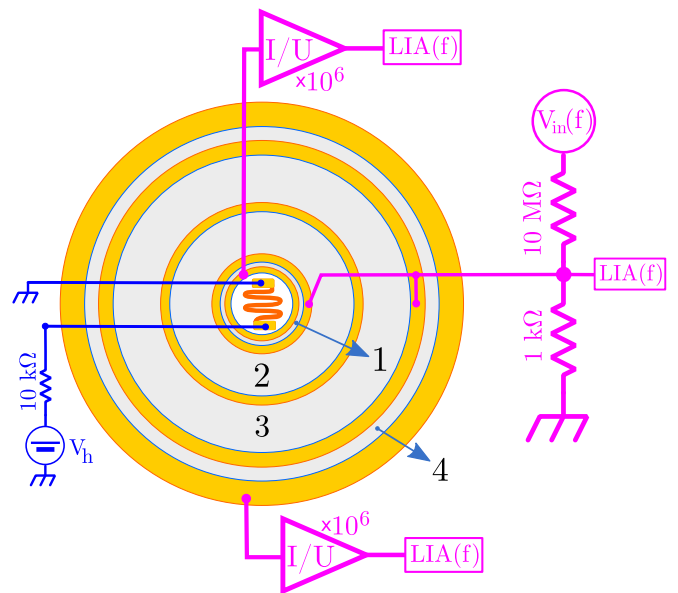


FIG. SM.3. The setup used to determine the temperature distribution is the same as the one used for conductance measurements. But in this case the heater is used to induce a temperature gradient in the sample. The conductance is recorded at the innermost and the outermost rings of the sample, ring 1 and 4. Notice that power is applied from a DC voltage source in the present case.

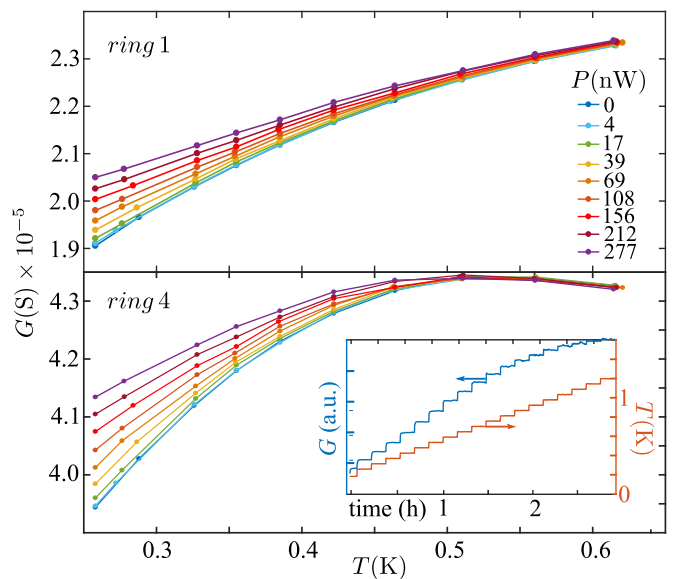


FIG. SM.4. Conductances of the rings 1 and 4 for different temperatures of the bath T and power injected at the heater P . Each set (color) corresponding to a different DC power applied to the heater, see SM text for details. The upper panel corresponds to the inner ring 1, while the lower one corresponds to the outer one ring 4. The lines between points improve readability. Inset: an example of raw measurements of conductance and temperature as functions of time at a fixed power of the heater.

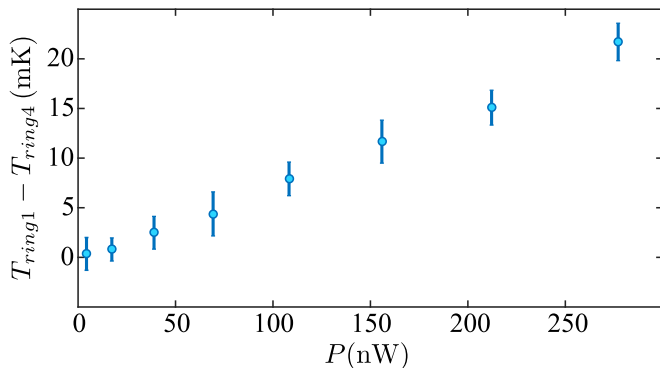


FIG. SM.5. Difference between the mean local temperatures of the rings 1 and 4, as a function of the power applied to the heater. It is obtained from the previous Fig. following the procedure described in Sec. IC.

conductance $G = e^2 \mathcal{L}_{11}/T$ and the Seebeck coefficient $S = \mathcal{L}_{12}/\mathcal{L}_{11}$ are fully determined by the transmission function $\mathcal{T}(\varepsilon)$, as indicated in Eq. (2) of the main text. We consider two regimes, depending on the intensity of the magnetic field to model $\mathcal{T}(\varepsilon)$, which we describe below.

1. Low magnetic field

For low magnetic fields, we consider the model introduced in Ref. 5 and 6. The transmission function reads

$$\mathcal{T}(\varepsilon) = \Lambda \sum_{n,\sigma} \frac{(n+1)\omega_c^2}{8\pi\hbar} A_{n,\sigma}(\varepsilon) A_{n+1,\sigma}(\varepsilon), \quad (5)$$

where Λ is a geometric factor relating the conductance to the conductivity, while $A_{n,\sigma}(\varepsilon) = \text{Im}[G_{n,\sigma}(\varepsilon)]$, being $G_{n,\sigma}(\varepsilon) = [\varepsilon - \varepsilon_{n,\sigma} - \Sigma(\varepsilon)]^{-1}$ the Green function calculated within the self-consistent Born approximation. $\varepsilon_{n,\sigma} = \hbar(n+1/2)\omega_c \pm \mu_B B/2$ is the energy of the Landau levels, including the Zeeman splitting, with \pm corresponding, respectively, to $\sigma = \uparrow, \downarrow$. Here, μ_B is the Born magneton, $\omega_c = eB/m^*$ is the cyclotron frequency, and $m^* = 0.067m_e$ is the effective mass of the electrons in the structure and m_e is the electron mass. The effect of disorder due to impurities introduces a widening Γ in the Landau levels, which is accounted for the self-energy $\Sigma(\varepsilon) = (\omega - \varepsilon_L)/2 - i\Gamma\sqrt{1 - (\varepsilon - \varepsilon_L)^2/(4\Gamma^2)}$. Here ε_L is the energy of the Landau level which is closest to ε . This model has two fitting parameters: Λ and Γ , which we adjust to fit the data of the conductance G , through Eq. (2) of the main text. This model fails to reproduce

$G(B)$ for high magnetic fields ($B > 1$ T in the sample shown in the main text).

2. High magnetic field

For higher magnetic fields, satisfying $k_B T \ll \hbar\omega_c$, and $\Gamma \ll \hbar\omega_c$, we can infer the transmission function more efficiently from the behavior of the conductance within a range of magnetic fields in the neighborhood of a given filling fraction ν . Notice that in the limit of $T \rightarrow 0$, the derivative of the Fermi function entering Eq. (2) of the main text, has the following behavior, $-\partial f(\varepsilon)/\partial\varepsilon \rightarrow \delta(\varepsilon - \mu)$. Therefore, for low temperatures, such that $k_B T \ll \hbar\omega_c$, we have

$$\mathcal{T}(\mu_\nu) \sim \frac{G(\mu_\nu)}{e}, \quad \mu_\nu = \frac{\hbar e B}{2m^*}, \quad B_{\nu+1} < B < B_\nu, \quad (6)$$

where $B_\nu = n_e h/(e\nu)$ is the magnetic field corresponding to the filling fraction ν , while μ_ν is the Fermi energy for the range of B within two consecutive integer filling factors.

B. Theoretical estimate of ΔT

From the behavior of the conductance we can infer the transmission function $\mathcal{T}(\varepsilon)$ as explained before, from where we can calculate the Onsager coefficients \mathcal{L}_{ij} . We recall that the thermovoltage is defined as follows

$$V_{tp}(B, t) = -S(B) \frac{\Delta T(t)}{T}, \quad (7)$$

where $S(B) = \mathcal{L}_{12}(B)/\mathcal{L}_{11}(B)$ is the Seebeck coefficient and we explicitly indicate that the response is a function of the time t . We also recall that the present experimental setup measures the component $V_{tp,2}$ of Eq. (4). Therefore, given the calculation of $S(B)$, we need to adjust the parameter $(\Delta T)_2/T$ in order to fit the data. Since the latter enters as the slope in the linear function $V(S)$, we analyze plots of the measured $V_{tp,2}$ vs the calculated S for values of B within which the Landau levels are partially filled and we fit a linear function to obtain the slope. Examples are shown in Fig. SM.6 for two different Landau levels, with bath temperature $T = 269$ mK and a power of 277 nW.

The corresponding fits cast $(\Delta T)_2 = (1.01 \pm 0.06)$ mK in the region from $B = 2.21$ T to 2.46 T (upper panel), and $(\Delta T)_2 = (1.33 \pm 0.06)$ mK in the region from $B = 2.625$ T to 3 T (lower panel), with uncertainties corresponding to a 95% confidence probability. Also notice that the intercept, which was taken as a free parameter of the regression is zero within the error in both cases.

¹ P. Märki, B.A. Braem, and T. Ihn, Rev. Sci. Instrum. **88**, 085106 (2017); doi:10.1063/1.4997963

² R.B. Laughlin, Phys. Rev. B **23**, 5632 (1981)

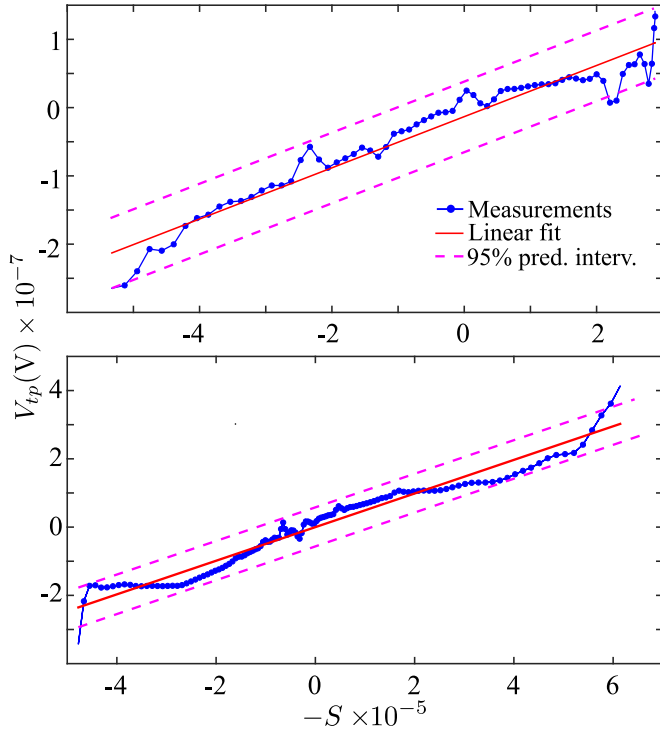


FIG. SM.6. Measured $V_{tp,2}$ signal *vs* calculated $-S$ within the range of fields $B = 2.21$ T to 2.46 T (upper panel) and $B = 2.625$ T to 3 T (lower panel). The slope of this relation is $(\Delta T)_2/T$.

³ S. Kobayakawa, A. Endo, and Y. Iye, J. Phys. Soc. Japan **82**, 053702 (2013)

⁴ W. E. Chickering, J. P. Eisenstein, L. N. Pfeiffer, and K. W. West, Phys. Rev. B **87**, 075302 (2013)

⁵ Y. Barlas and K. Yang, Phys. Rev B **85**, 195107 (2012)

⁶ M. Jonson and S. M. Girvin, Phys. Rev. B **29**, 1939 (1984)

⁷ J. Martin, S. Ilani, B. Verdene, J. Smet, V. Umansky, D. Mahalu, D. Schuh, G. Abstreiter, A. Yacoby, Science **305**, 980 (2004)

⁸ A. V. Kavokin, B. L. Altshuler, S. G. Sharapov, P. S. Grigoryev, A. A. Varlamov, PNAS **117**, 2846 (2020)